IOPscience iopscience.iop.org

Home Search Collections Journals About Contact us My IOPscience

Statistical properties of charged interfaces

This article has been downloaded from IOPscience. Please scroll down to see the full text article.

2002 J. Phys.: Condens. Matter 14 7811

(http://iopscience.iop.org/0953-8984/14/34/303)

View the table of contents for this issue, or go to the journal homepage for more

Download details:
IP Address: 171.66.16.96
The article was downloaded on 18/05/2010 at 12:25

Please note that terms and conditions apply.

INSTITUTE OF PHYSICS PUBLISHING JOURNAL OF PHYSICS: CONDENSED MATTER

J. Phys.: Condens. Matter **14** (2002) 7811–7834 PII: S0953-8984(02)36542-1

Statistical properties of charged interfaces

S Teber

Laboratoire de Physique Théorique et Modèles Statistiques, Bâtiment 100, Université Paris-Sud, 91406, Orsay-Cédex, France

Received 2 May 2002
Published 15 August 2002
Online at stacks.iop.org/JPhysCM/14/7811

Abstract

We consider the equilibrium statistical properties of interfaces submitted to competing interactions: a long-range repulsive Coulomb interaction inherent to the charged interface and a short-range, anisotropic, attractive one due to either elasticity or confinement. We focus on one-dimensional interfaces such as strings. Model systems considered for applications are mainly aggregates of solitons in polyacetylene and other charge-density wave systems, domain lines in uniaxial ferroelectrics and the stripe phase of oxides. At zero temperature, we find a shape instability which leads, via phase transitions, to tilted phases. Depending on the regime, elastic or confinement, the order of the zero-temperature transition changes. Thermal fluctuations lead to a pure Coulomb roughening of the string, in addition to the usual one, and to the presence of angular kinks. We suggest that such instabilities might explain the tilting of stripes in cuprate oxides. The three-dimensional problem of the charged wall is also analysed. The latter experiences instabilities towards various tilted phases separated by a tricritical point in the elastic regime. In the confinement regime, the increase of dimensionality favours either the melting of the wall into a Wigner crystal of its constituent charges or a strongly inclined wall which might have been observed in nickelate oxides.

1. Introduction

Various types of systems display peculiar properties due to competing long-range forces. In this paper we focus on the statistical properties of charged interfaces, in Ising-like systems, such as aggregates of charged topological defects in charge-density wave (CDW) systems [1, 2] and among them polyacetylene [3], charged domain lines in uniaxial ferroelectrics [4] or stripes in oxides [5, 6]. Instabilities, such as the observed inclination of stripes in cuprates [7] and manganese [8], might be related to the presence of the long-range Coulomb interaction and its competition with an attractive force. Uniaxial ferroelectrics and density waves are also model systems where such instabilities could take place. The present study deals with one-dimensional (1D) or two-dimensional (2D) charged interfaces, i.e. strings or walls. The former are realized in oxides,

 © 2002 IOP Publishing Ltd Printed in the UK

monolayers of doped conducting polymers or other CDWs and junctions in field-effect experiments [9] for equivalent materials. The latter might be present in the systems cited above, due to a dimensional crossover which induces a three-dimensional (3D) ordering.

The above interests have emerged from a model-independent theory concerning the statistics and thermodynamics of uncharged [10] and charged [11] solitons. The system considered is twofold degenerate and, when topologically doped, the solitons form a one-component plasma in either 2D or 3D space. The competition between the long-range 3D Coulomb interaction of the particles and the confinement force between them has led to a very rich phase diagram. Particularly interesting is the regime where the temperature is much less than the confinement energy scale, so that the solitons are actually bound into pairs, and the repulsive Coulomb interaction is weak enough to preserve these bisolitons as the elementary particles. In this regime, aggregated phases of bisolitons have been shown to exist. The study of such aggregates in the continuum limit is equivalent to the study of charged interfaces.

The statistical properties of charged fluctuating manifolds have been considered previously [12]. In this study, the authors have considered a generalization of the theory of polyelectrolytes, cf [13], and have focused on the properties emerging from scale invariance and renormalization. Even though some of our results converge with the previous study, which seems to be quite natural, our aim is different. We consider interfaces directed along an anisotropy axis of the system which are either in an elastic or confinement regime; the latter is relevant to quasi-1D systems in relation to the statistics of solitons mentioned above. In both regimes, the Coulomb interaction favours the disintegration of the interface. In contrast with the instability towards a modulation which has been suggested in [11], this competition, as we show, leads to zero-temperature shape instabilities with respect to a tilting of the interface. We focus mainly on the properties related to this discrete symmetry breaking. This enables us to better understand the structure of the solitonic lattice in the presence of the long-range repulsive interaction. In this respect, and as explained in [11], even though this problem seems to be quite old, the detailed impact of the Coulomb interaction has not been reported previously. Moreover, charged solitonic lattices are commonly observed nowadays as stripes in various oxides. Experimentally the observation, that upon doping the system, at low temperatures, a transition from a collinear, i.e. vertical, to a diagonal stripe phase takes place [7], is strikingly similar to our actual results.

The paper is organized as follows. We mainly concentrate on the statistics of a charged string. In section 2 we present the models of the confined and elastic charged strings. In section 3 we derive the statistics of the string with the help of a saddle-point calculation. We present the zero-temperature results dealing with the instabilities of the string. In section 4 the effects of thermal fluctuations are considered. In section 5 the previous results are confirmed with the help of a numerical approach. In section 6.1 the present study is applied to the 2D and 3D solitonic lattices, as well as stripes and uniaxial ferroelectrics.

2. Elastic and confinement regimes for the charged string

The problem of the charged string [11] has emerged from the study of the statistics of topological defects, i.e. solitons, common to CDW systems. These general arguments are reproduced in the following as they give a full meaning to the physical origins of the present theory; see [1] for a review on the physics of topological defects in CDW systems. It should, however, be clear that this study is also relevant to other systems with discrete symmetry breaking, as has been mentioned already in the introduction.

For the moment, we consider a 1D system, i.e. a single chain, in a CDW state. The latter is described by a lattice order parameter which is complex in general

$$\Delta(x) = |\Delta(x)| \exp(\mathrm{i}\varphi(x))$$

where x runs along the chain, $|\Delta(x)|$ is related to the CDW gap and $\varphi(x)$ fixes the position of the CDW with respect to a host lattice. In a weakly commensurate CDW the low-energy excitations are excitations of the phase. This leads, cf [14], to a sine-Gordon-type Hamiltonian

$$H = \int \mathrm{d}x \left(\frac{\hbar v_F}{2\pi} \left(\frac{\partial \varphi}{\partial x} \right)^2 - W \cos(M\varphi) \right) \tag{1}$$

where the first term gives the elastic energy of the CDW and the second term reflects the pinning of the CDW superstructure by the host lattice; M is the degeneracy of the ground state.

The non-trivial solutions of the equation of motion associated with (1) are the solitons, i.e. the φ particles [15], which may be viewed as compressions or dilatations of the CDW. As we are in the realm of electronic crystals, the solitons might therefore carry a charge which is fractional, i.e. $q = 2/M$, in the general case. For a double-degenerate ground state, $M = 2$, these are given by

$$\varphi(x) = 2 \arctan(\exp(2x/\xi)) \tag{2}$$

where the length $\xi \sim \sqrt{\hbar v_F / W}$ corresponds to the width of this nucleus domain wall connecting the two ground states $\varphi(\pm\infty) = \pm 1$.

The situation is slightly different for the twofold degenerate trans-polyacetylene because in this case the band is half-filled and the system is commensurate. In particular, equation (1) does not describe this case. However, the previous arguments remain qualitatively the same. The defect is an amplitude or π soliton; it carries an integer charge and is described by

$$\Delta(x) = \Delta_0 \tanh(x/\xi) \tag{3}$$

where Δ_0 is a constant deformation of the chains. Again this excitation connects the two ground states of the system $\Delta(\pm\infty) = \pm\Delta_0$.

For a quasi-1D system, which we consider here, neighbouring chains must have the same phase modulo 2π. This leads to the following general two-particle interaction

$$E(\delta x) = -V \int \mathrm{d}z \, \Delta_\alpha(\delta x - z) \Delta_\beta(z) \tag{4}$$

between neighbouring chains α and β, with coupling constant V, and solitons distant by δx. In the coarse-grained regime, $\delta x \gg \xi$, interaction (4) grows linearly, $E \approx V \delta x$, a signature of the confinement of the defects. This can be shown explicitly with the help of equations (3) and (4). Dealing with a string, e.g. a domain line of solitons, this confinement energy is equivalently reproduced by the solid-on-solid (SOS) model. The related Hamiltonian reads

$$H_{conf} = \frac{J_\perp}{a_y} \sum_{y=0}^{L-1} |x_{y+1} - x_y| \tag{5}$$

where we have taken $J_\perp = V a_y$ as the inter-chain energy scale, y runs along the vertical direction and x_y is an integer variable giving the deviation of the string with respect to the y-axis.

The opposite case, corresponding to small deviations $\delta x \ll \xi$, is more general for the energy then increases quadratically $E \approx V \delta x^2$. This is equivalent to the elastic model which is extensively used in interface physics. The related Hamiltonian reads

$$H_{elast} = J_\perp \int \frac{\mathrm{d}y}{a_y} \left(\frac{\mathrm{d}x}{\mathrm{d}y} \right)^2. \tag{6}$$

These two interface models are well known [16]. To compactify notations, we define

$$H_{0p} = J_\perp \int \frac{\mathrm{d}y}{a_y^p} \left| \frac{\mathrm{d}x}{\mathrm{d}y} \right|^p \tag{7}$$

where $p = 1, 2$ leading respectively to the confinement and elastic regimes, and where the continuum limit has been taken in both cases. We thus see that a crossover (corresponding to fractional $1 < p < 2$) from the elastic to the confinement regime takes place as the distance between solitons increases, i.e. as the tilt angle of the string increases. This is manifested by the fact that $\delta x = (\mathrm{d}x/\mathrm{d}y)a_y = \zeta a_y$ where ζ is related to the tilt angle of the string and a_y is the inter-chain distance. For $\zeta \ll \xi/a_y$ the string is elastic whereas for $\zeta \gg \xi/a_y$ the confined string is relevant. The crossover between the two regimes takes place at

$$\zeta_0 = \xi/a_y. \tag{8}$$

The introduction of the 3D long-range Coulomb interaction yields

$$H_c = \frac{(ze)^2}{2\epsilon} \int\int \mathrm{d}y\, \mathrm{d}y' \left(\frac{1}{\sqrt{(y-y')^2 + (x(y) - x(y'))^2}} - \frac{1}{\sqrt{(y-y')^2}} \right) \tag{9}$$

where $z \leqslant 1$ so that the elementary constituent of the string might carry a fractional charge ze ($z = 1$ for polyacetylene), ϵ is the dielectric constant of the isotropic, neutral medium in which the plane is embedded and the contribution of the vertical string has been subtracted.

The thermodynamics of the charged interface is governed by $H_p = H_{0p} + H_c$ or explicitly

$$H_p = J_\perp \int \frac{\mathrm{d}y}{a_y^p} \left| \frac{\mathrm{d}x}{\mathrm{d}y} \right|^p + \frac{(ze)^2}{2\epsilon} \iint \mathrm{d}y\, \mathrm{d}y' \left(\frac{1}{\sqrt{(y-y')^2 + (x(y) - x(y'))^2}} - \frac{1}{|y-y'|} \right). \tag{10}$$

3. The charged string at zero temperature

3.1. The saddle-point approximation

We consider a configuration

$$x(y) = x^{(0)}(y) + \delta x(y) \tag{11}$$

where $x(y)$ has been expanded in the vicinity of the saddle-point distribution $x^{(0)}(y)$ with deviations $\delta x(y)$. Free boundary conditions are taken. The expanded Hamiltonian reads, in the harmonic approximation

$$H_p = H_p^{(0)} + \tfrac{1}{2} \iint \mathrm{d}y\, \mathrm{d}y'\, \delta x(y) \delta^{(2)} H / \delta x(y) \delta x(y')|_{\delta x = 0} \delta x(y') + \cdots \tag{12}$$

where H_p is given by equation (10) and $H_p^{(0)} \equiv H_p\{\delta x^{(0)}(y)\}$. The saddle-point distribution is given by $\delta H_p / \delta x(y) = 0$, that is

$$J_\perp p (\Delta x^{(0)}(y))^{p-1} = \frac{(ze)^2}{2\epsilon} \int_{-\infty}^{+\infty} \mathrm{d}y' \frac{x^{(0)}(y') - x^{(0)}(y)}{((y-y')^2 + (x^{(0)}(y) - x^{(0)}(y'))^2)^{3/2}}. \tag{13}$$

This non-linear integro-differential equation cannot be solved exactly. We therefore take an ansatz for the ground-state configuration $x^{(0)}(y)$ of the string. As can be seen from equation (10), at zero temperature, the elastic or confinement term favours a vertical string, i.e. along the y-axis, whereas the Coulomb favours the disintegration of the string in the perpendicular direction. Instabilities of the string arise from the competition between these interactions. We find that these instabilities lead to a tilted string as the new ground state of the system. Therefore

$$x^{(0)}(y) = \zeta y \tag{14}$$

where $\zeta = \tan\theta$, θ being the tilt angle of the string with respect to the y-axis. This ansatz satisfies the linearized equation (13) up to some logarithmic corrections. As is shown explicitly in the following, ζ is related to the ratio between the Coulomb and confinement or elastic energy scales. It is thus related to the elementary charge of the string constituent soliton.

With the help of equations (14) and (10), equation (12) reads

$$H_p = H_p^{(0)} + \sum_k \lambda_{p,k}^2(\zeta_p)|\delta x_k|^2 \tag{15}$$

with the eigenvalues

$$\lambda_{p,k}^2(\zeta_p) = k^2 J_\perp \left(p(p-1) + \frac{2\zeta_p^2 - 1}{[1+\zeta_p^2]^{\frac{5}{2}}}\gamma(k) \right). \tag{16}$$

ζ_p is the optimal angle corresponding to the distribution (14) minimizing $H_p^{(0)}$ and

$$\gamma(k) = \gamma \log(1/ka) \tag{17}$$

with

$$\gamma = \frac{w_y}{J_\perp} \qquad w_y = \frac{(ze)^2}{2\epsilon a_y}, \tag{18}$$

where γ is the ratio of the Coulomb energy scale w_y to the elastic or confinement energy scales.

The first term in equation (15) corresponds to the mean-field Hamiltonian. $H_p^{(0)}$ leads to the following mean-field free energy density

$$f_p^{(0)}(\zeta) = \frac{J_\perp}{a_y}\left[\zeta^p + \gamma_D \left(\frac{1}{\sqrt{1+\zeta^2}} - 1 \right) \right] \tag{19}$$

where $\gamma_D = \gamma(l_D^{-1})$ and l_D is the Debye screening length taken into account as a hard cut-off to eliminate the logarithmic divergence of the Coulomb term in the thermodynamic limit. Details concerning the screening mechanisms and the expressions of l_D are reported in appendix A. As can be seen in the first term of equation (19) in the confinement regime, the absolute value has been dropped. This is the non-return approximation for the confinement regime, the limitations of which are considered at the end of this section. In the following subsections, we see how the tilted phase arises via zero-temperature phase transitions in both $p = 1, 2$ regimes.

3.2. The elastic charged string

We first consider the elastic regime, with $p = 2$ in equation (19), corresponding to tilt angles below the crossover value (8). Figure 1 displays this free energy as a function of the angle. Until

$$\gamma_D^c = 2 \tag{20}$$

the vertical line, $\zeta_2 = 0$, is stable. Above γ_D^c the vertical line becomes unstable and the free energy has a double well shape. This is due to the double degeneracy of the system; the new, tilted, ground states corresponding to $\pm\zeta_2$ have the same energies. The optimal angle reads

$$\zeta_2 = \sqrt{\left(\frac{\gamma_D}{2}\right)^{\frac{2}{3}} - 1}. \tag{21}$$

The transition at γ_D^c is of the second order. This can be shown by evaluating a quantity analogous to the heat capacitance in usual thermodynamic phase transitions; that is

$$C_\gamma = -\gamma_D \frac{\partial^2 f_2^{(0)}}{\partial \gamma_D^2} \tag{22}$$

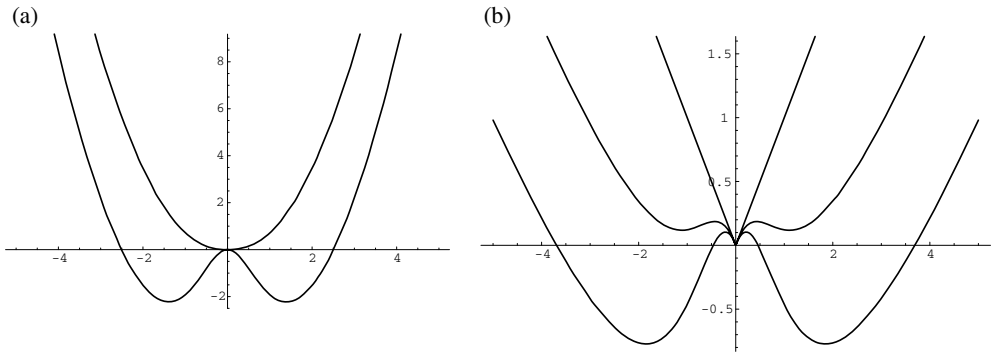

Figure 1. (a) Mean-field free energy of the elastic string (19) as a function of ζ exhibiting a second-order phase transition. The two curves correspond to $\gamma_D < \gamma_D^c$, where the vertical string is stable, and $\gamma_D > \gamma_D^c$, where the tilted line is stable as can be seen from the double well. (b) Free energy of the confined string as a function of ζ exhibiting a first-order transition from the vertical string to the free string. From upper to lower curves: free model $\gamma_D = 0$, metastable states appear when $\gamma_D > \gamma_D^*$, and these become stable states when $\gamma_D > \gamma_D^c$.

with the tilt angle given by equation (21) above the transition and vanishing below. Equation (22) yields

$$C_\gamma = \frac{2J_\perp}{9}\left(\frac{2}{\gamma_D}\right)^{2/3}\left[1+\frac{1}{2}\left(\frac{\gamma_D}{2}\right)^{1/3}\right] \qquad \gamma_D > \gamma_D^c$$

and $C_\gamma = 0$ otherwise, which leads to a jump at the transition, $\Delta C_{\gamma_D^c} = J_\perp/3$.

The linear stability analysis of these mean-field solutions can be performed by looking at equation (16) with $p = 2$

$$\lambda_{2,k}^2(\zeta_2) = J_\perp k^2\left(2+\frac{2\zeta_2^2-1}{[1+\zeta_2^2]^{\frac{5}{2}}}\gamma(k)\right). \tag{23}$$

These eigenvalues must be positive, for all momentum k, in order to ensure the stability of the solution.

Expanding first around the vertical line, $\zeta_2 = 0$, equation (23) leads to the following stability criterion

$$\gamma(k) = \gamma\log(1/ka) < 2, \qquad \forall k$$

or

$$k > k_c = \frac{1}{a}\exp(-2/\gamma_0)$$

where k_c is the Coulomb-dependent critical momentum. This shows that the instability is driven by low-momentum, i.e. long wavelength, modes. Noting that $1/l_D < k < 1/a$, we find, in agreement with the mean-field analysis, that the vertical string is stable as long as $k_c < 1/l_D$. $k_c = 1/l_D$ returns us to equation (20). Increasing the strength of the Coulomb interaction increases k_c. For $k_c s > 1/l_D$ a continuous set of modes, i.e. between $1/l_D$ and k_c, has negative eigenvalues so that the vertical string is no longer stable.

Expanding around $\xi_2 \neq 0$, we see from equation (23), that all modes are stable as soon as $\xi_2 > 1/\sqrt{2}$. For such tilt angles, we are of course above the critical point, as can be seen with the help of equation (21). The tilted line is thus stable against harmonic fluctuations.

3.3. The charged string in the confinement regime

When ζ becomes larger than the crossover value $\zeta > \zeta_0$, cf (8), the elastic approximation is no longer valid and we reach the peculiar confinement regime with $p = 1$. In this case, the eigenvalues (16) are given by

$$\lambda_{1,k}^2(\zeta_1) = J_\perp \frac{2\zeta_1^2 - 1}{[1+\zeta_1^2]^{\frac{5}{2}}} k^2 \gamma(k). \tag{24}$$

We see from equation (24) that configurations with $\zeta_1 > 1/\sqrt{2} = \zeta_1^*$ are always stable against harmonic fluctuations. Moreover, this is a pure Coulomb stability. On the other hand, configurations with $\zeta_1 < 1/\sqrt{2} = \zeta_1^*$ are always unstable. This implies that the stability of the vertical string cannot be analysed within the present model. This is related to the non-return approximation made in equation (15). However, numerical simulations show that the tilted string is, here also, the new ground state, cf section 4. In relation to the crossover between elastic and confinement regime, we can then interpret ζ_1^* as a low boundary for the crossover angle ζ_0, cf (8). In the following, we thus consider solutions corresponding to $\zeta_1 > \zeta_1^*$, i.e. $\gamma_D > \gamma_D^*$.

Figure 1 shows a crucial difference between the confinement and elastic regimes concerning the mechanism by which tilted strings, i.e. a double well in the free energy, appear. In contrast to the previous case, the second derivative of the energy remains positive a signature of the fact that the correlation length remains finite and that the transition is first order in the confinement regime. Metastable states thus appear. We first show that they appear at γ_D^*, the upper spinodal strength. From equation (19) with $p = 1$, the vanishing of the first derivative of the free energy density leads to

$$1 = \gamma_D \frac{\zeta_1}{(1+\zeta_1^2)^{3/2}}. \tag{25}$$

The spinodal line, above which (metastable) solutions appear, can be defined with the help of the coupled equation (25) and its derivative. This leads to

$$\zeta_1^* = \frac{1}{\sqrt{2}} \qquad \gamma_D^* = \frac{3\sqrt{3}}{2} \approx 2.6. \tag{26}$$

Increasing the Coulomb interaction we reach the critical regime where the mean-field free energy of the tilted solution becomes equal to that of the $\zeta = 0$ solution $f_1(\zeta = 0) = f_1(\zeta_1)$. Equations (25) and (26) define the critical point and lead to

$$\zeta_1^c = \sqrt{\frac{1}{2} + \frac{\sqrt{5}}{2}} \approx 1.3 \qquad \gamma_D^c \approx 3.3. \tag{27}$$

As in critical phenomena, for $\gamma_D > \gamma_D^c$, the system jumps to the non-zero tilt angle solution corresponding to the absolute minimum of the energy.

3.4. Quantum fluctuations

At $T = 0$ the string is submitted to quantum fluctuations. These give a contribution to the difference correlation function of the form

$$\langle \delta x(y)^2 \rangle \approx \hbar \log y,$$

where y is along the string. Assuming that the distance between lines is of the order of l_D, collisions between lines will take place on a scale $y \approx \exp l_D$ due to these transverse fluctuations. These collisions are thus present on scales much larger than our upper cut-off l_D and will therefore not affect previous results.

4. The charged string at finite temperature

In this section, we look for the effect of temperature. In the following we consider the low-temperature regime where the string needs to be quantized. Thermodynamic quantities can be evaluated from the expression of the full free energy. We give the expression of the heat capacitance. In the presence of thermal fluctuations, the angular degeneracy gives rise to defects connecting the ground states of the string: the angular kinks. The N-kink problem is defined and the energies of the one-kink and two-kink string configurations are given. Single angular kinks are activated. Bi-angular kinks are non-topological and are subject to a Coulomb confinement; these excitations correspond to a Coulomb roughening of the string in addition to the usual roughening.

4.1. Thermodynamic quantities

Apart from a logarithmic correction the spectrum (16) is that of phonons, a feature of the saddle-point approximation. We thus have a harmonic oscillator problem which is easily quantized

$$E_{\{n_k\}} = E^{(0)} + \sum_k (n_k + \tfrac{1}{2})\omega_{k,p}$$

where the units have been chosen such that $\omega_{k,p}$ has the dimension of an energy.

This yields

$$f_p = f_p^{(0)} + T\int_{\frac{1}{l_D}}^{\frac{1}{a}} \frac{\mathrm{d}k}{2\pi} \log(1 - \exp(-\omega_{k,p}/T)) \tag{28}$$

where the second term is an entropic contribution and the zero point energy has been included in the first term. The general expression of the free energy density is then

$$f_p = f_p^{(0)} - \frac{T^2}{12\sqrt{J_\perp[p(p-1)+\gamma(\zeta)]}} \tag{29}$$

where

$$\gamma(\zeta) = \gamma \frac{2\zeta^2 - 1}{(1+\zeta^2)^{5/2}}$$

and γ_0 is given by equation (18).

It is simple, from equation (29), to compute the heat capacitance, at constant length, of the system. We obtain

$$C_L^{(p)} = \frac{T}{6\sqrt{J_\perp\left[p(p-1)+\gamma\frac{2\zeta^2-1}{(\zeta^2+1)^{5/2}}\right]}} \tag{30}$$

which is linear in T with an angle-dependent coefficient. Such an expression can be usefully compared with experimental work on related physical systems.

4.2. Excited states of the string

4.2.1. The angular kink solution. Coarse graining the system, we consider the kink as a point-like excitation as in figure 2(b). This amounts to neglect of its core on the scale of which elastic or confinement energy compete with the Coulomb energy to connect smoothly the two ground states as shown in figure 2(a). At finite temperatures, a general configuration of the string is thus similar to figure 2(c) where an array of angular kinks is present. This shape agrees with the numerical results displayed in figure 2(d).

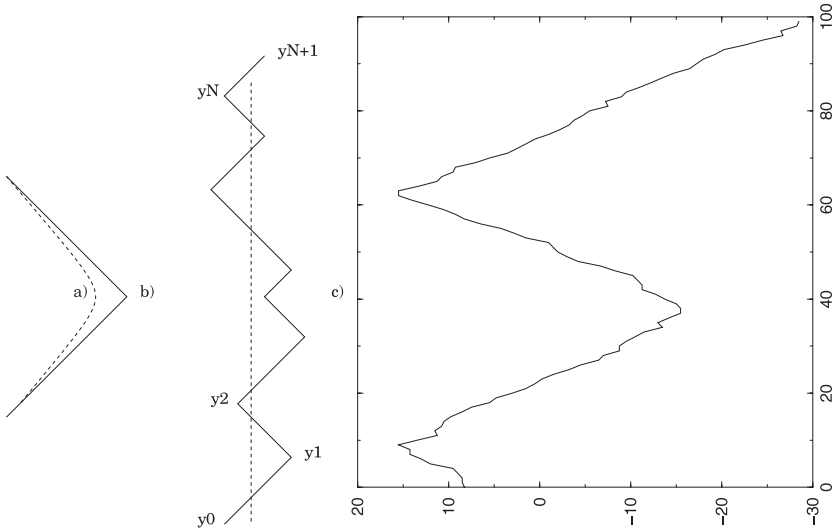

Figure 2. Angular kink shapes: (a) exact kink shape; (b) point-like kink; (c) shape of the string with N-kink excitations; (d) numerical result.

The energy of an array of N-kinks is given by

$$\Delta E_N = \frac{w_y}{a_y} \sum_{i,j=0}^{N} \int_{y_i}^{y_{i+1}} \mathrm{d}y \int_{y'_j}^{y'_{j+1}} \mathrm{d}y' \frac{1}{\sqrt{(y-y')^2 + (x_{i+1}(y) - x_{j+1}(y'))^2}} - E_N^{(0)} \tag{31}$$

where w_y has been defined in equation (18), $y_{N+1} = -y_0 = +\infty$ with the other y_i denoting the positions of the defects, $x_i(y)$ is a portion of string connecting point y_{i-1} to point y_i, and $E_N^{(0)}$ is the Coulomb energy of the same string without kinks, i.e. at $T = 0$. The point-like kink approximation amounts to use of the tilted ansatz ground state $x_i(y) = (-1)^i \zeta (y - y_i) + x_i(y_i)$. Equation (31) is available for both elastic and confinement models. This is consistent with the fact that these models have similar long distance properties, as shown in appendix B with the help of a transfer matrix approach. However, even though exact results can be obtained with the help of equation (31) within the limits of the point-like kink approximation, the obtained expressions, in the general case, are quite intractable. We therefore consider simple cases.

Firstly, the one-kink energy reads

$$\Delta E_1 = \frac{L w_y}{a_y \sqrt{1+\zeta^2}} \ln\left[\frac{1+\sqrt{1+\zeta^2}}{2}\right] \tag{32}$$

where L is the length of the string. The energy of the kink is lower than the total energy of the string which is over-extensive in the absence of screening, i.e. $\sim L \log L$. Nevertheless, equation (32) shows that the kink has infinite energy in the thermodynamic limit, a special feature of the long-range Coulomb interaction. In the presence of screening, the energy of the string becomes extensive, i.e. $\sim L \log l_D$, and the single angular kink is activated

$$\Delta E_1^D = \frac{l_D w_y}{a_y \sqrt{1+\zeta^2}} \ln\left[\frac{1+\sqrt{1+\zeta^2}}{2}\right].$$

Thus, we have an exponentially small density of kinks

$$n \approx \exp\left(-\frac{\Delta E_1^D}{T}\right). \tag{33}$$

4.2.2. Transverse fluctuations. Given the density of kinks (33), the length of the string between two angular kinks is given by

$$l \approx \frac{1}{n}.$$

Within this length, thermal fluctuations also play an important role. With the help of equation (15), in the limit of large y the difference correlation function reads

$$\langle(\delta x(y) - \delta x(0))^2\rangle_p \approx y\frac{Ta_y}{J_\perp}\frac{1}{p(p-1)+\gamma(\zeta)\ln(y/a)} \tag{34}$$

where we have omitted higher-order terms. Equation (34) shows that the charged string, which might be tilted if the Coulomb interaction is sufficiently strong, roughens at all non-zero temperatures. This roughening has two origins: there is a usual roughening due to the elasticity of the string and a Coulomb roughening, originating from the spontaneous symmetry breaking. Hence, there is no positional order

$$\langle\delta x\rangle \sim \sqrt{\langle(\delta x(y) - \delta x(0))^2\rangle_p} \approx \sqrt{y} \to \infty \qquad y \to \infty$$

but there is long-range orientational order

$$\langle\delta\zeta\rangle \sim \frac{\mathrm{d}\langle\delta x\rangle}{\mathrm{d}y} \approx 1/\sqrt{y} \to 0 \qquad y \to \infty.$$

Notice that the screened Coulomb interaction does not affect the value of the roughening exponent which is $1/2$. This is also known from a theory of fluctuating charged manifolds, cf [12], as has been said in the introduction, and confirms the validity of our approach. What is peculiar to our system is the Coulomb roughening of the string due to the spontaneous symmetry breaking. The latter might be isolated from the usual roughening by the following procedure.

We consider the two-kink problem on the same lines as the single kink of the previous subsection. When their separation δy, along the axis of preferable orientation, is smaller than the screening length, equation (31) yields

$$\begin{aligned}\Delta E_2 = \frac{w_y}{a_y\sqrt{1+\zeta^2}}\sum_{\epsilon=\pm}\epsilon\\ \times\Bigg\{\delta y\log\Bigg(\frac{\sqrt{(1+\zeta^2)[(L+\delta y)^2+\zeta^2(L-\epsilon\delta y)^2]}+\ L+\delta y+\zeta^2(L-\epsilon\delta y)}{2\delta y\left[1+\zeta^2\frac{1-\epsilon}{2}\right]}\Bigg)\\ +\delta y\log\Bigg(\frac{\sqrt{(1+\zeta^2)[L^2+\zeta^2(L-\delta y-\epsilon\delta y)^2]}+L+\zeta^2(L-\delta y-\epsilon\delta y)}{2\delta y[1+\zeta^2\frac{1-\epsilon}{2}]}\Bigg)\\ +L\log\Bigg(\frac{\sqrt{(1+\zeta^2)[(L+\delta y)^2+\zeta^2(L-\epsilon\delta y)^2]}+L+\delta y+\zeta^2(\delta y-\epsilon L)}{2L[1+\zeta^2\frac{1-\epsilon}{2}]}\Bigg)\\ +(L-\delta y)\\ \times\log\Bigg(\frac{\sqrt{(1+\zeta^2)[L^2+\zeta^2(L-\delta y-\epsilon\delta y)^2]}+\ L+\zeta^2(\delta y-\epsilon(L-\delta y))}{2(L-\delta y)\left[1+\zeta^2\frac{1-\epsilon}{2}\right]}\Bigg)\Bigg\}.\end{aligned} \tag{35}$$

The term with $\epsilon = +1$ corresponds to the contribution of the kinked string whereas the one with $\epsilon = -1$ is the subtraction of the ground-state string. When $\delta y < l_D \ll L$, equation (35) yields

$$\Delta E_2 \approx \frac{\delta y w_y}{a_y\sqrt{1+\zeta^2}}\log(1+\zeta^2) + \mathrm{O}\left(\left(\frac{\delta y}{L}\right)^2\right). \tag{36}$$

In the limit $L \to \infty$ the angular bikink has a finite energy. At the optimal angle, equation (36) shows that this pair is confined with an energy growing linearly as a function of the transversal distance between the kinks. The proliferation of angular bikinks is therefore shown to be a signature of the Coulomb roughening of the charged string.

5. Numerical approach

The statistics of the charged string in both elastic and confinement regimes has been studied with the help of a Monte Carlo–Metropolis algorithm. These numerical simulations allow us to compute the properties of the full Hamiltonian (10) with open boundary conditions as above. The ground state is found with the help of a simulated annealing. The shape of the distribution, the value of the zero-temperature order parameter ζ and the energy of the distribution as a function of γ have been computed to detect the various instabilities and associated phase transitions. The effect of thermal fluctuations, i.e. the roughening and tunnelling, have also been studied. These numerical results show good agreement with the analytical results presented above.

5.1. Elastic string

We focus first on the zero-temperature properties of the string. The ground state has been found by performing a logarithmic simulated annealing during each Monte Carlo simulation

$$T[i] = T[0]\frac{\ln 2}{\ln(2+i)}$$

where i is the Monte Carlo step and $T[0]$ is a high initial temperature. Due to an improved algorithm to treat the Coulomb interaction, the logarithmic decay of the temperature has been successfully implemented in the simulations. As is well known, this leads to the ground state with the lowest probability of being trapped in metastable states.

We compute the properties of the full Hamiltonian (10). The numerical coupling constant in equation (9) is defined by γ_{num}. The rigidity $J_\perp$ in equation (6) is taken to be unity. With these numerical coupling constants, a comparison can be made with the analytical results obtained using a mean-field theory. In this respect γ_{num} should correspond to γ in equation (17). The computational cell must, of course, be finite and there is therefore no reason for using an upper cut-off limit l_D. Therefore, $l_D \to L$ and $\gamma_{num} = \gamma_{numD}/\ln L$ which reflects the non-extensivity arising from the long-range interaction. In particular, the critical numerical coupling constant should be given by $\gamma^c_{num} = \gamma^c_{numD}/\ln L$ where γ^c_{num} should be obtained by simulations and γ^c_{numD} compared with equation (20).

We consider first the behaviour of the order parameter ζ as a function of γ_{num} for different sizes L. A typical result is displayed in figure 3. Each point in this figure corresponds to an independent Monte Carlo simulation, i.e. given by generating a new random configuration which is then thermalized by the simulated annealing and brought to an effective zero temperature. Due to the double degeneracy of the ground state, it is the absolute value of ζ which has been plotted. The behaviour is that expected by the analytical results. Furthermore, the critical coupling constant given by γ^c_{Dnum} agrees with γ^c_D with an error of the order of 1% as is given by fitting the numerical data with equation (21). Below the transition, the mean angle is zero. A typical shape of the string in this region is given in figure 4. The string is vertical on average. Above the transition, the mean angle increases with γ_{num} in accordance with equation (21). The string is then tilted with respect to the main axis, as shown also in figure 4. No jump in the order parameter takes place, which is an indication that the phase

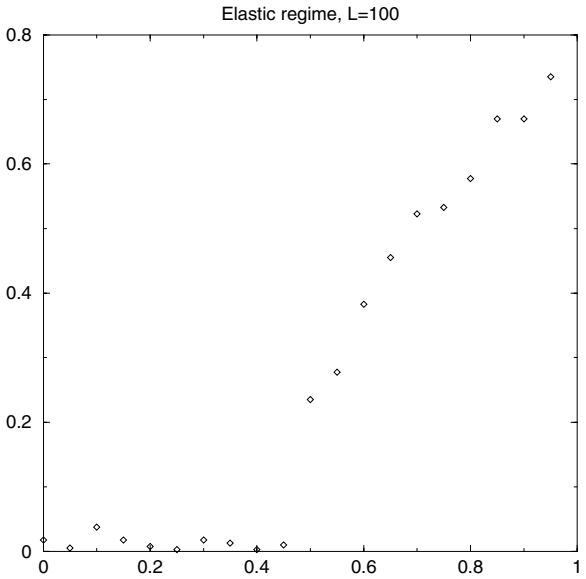

Figure 3. Absolute value of ζ as a function of γ_{num}.

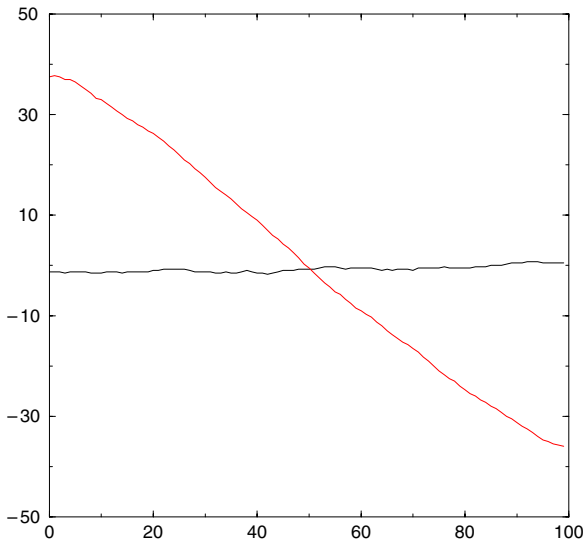

Figure 4. Shape of the string. Below the transition, the charged string is vertical; above the transition, it tilts away from the anisotropy axis.
(This figure is in colour only in the electronic version)

transition is second order. The energy of the string has however been computed as a function of γ_{num}. It is continuous. The second derivative is found, on the other hand, to diverge around the critical value.

Next we take into account thermal fluctuations. When the temperature is less than the activation energy of single angular kinks ΔE_1, cf (32), the line is rough as shown by figure 5.

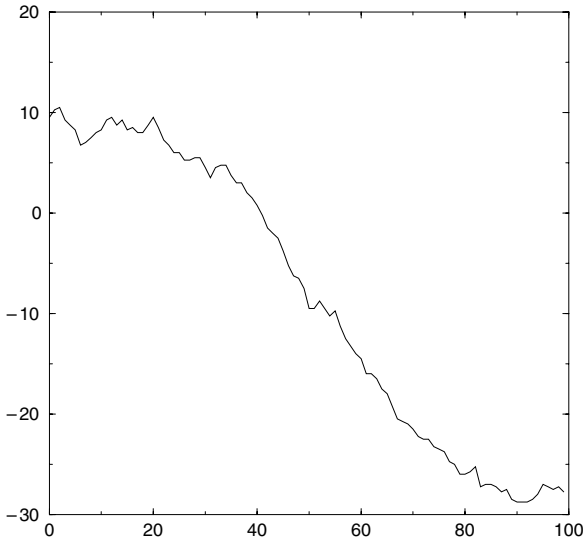

Figure 5. Rough inclined string at low temperature; the orientational order is preserved.

Above ΔE_1 single angular kinks are present in addition to the roughening, cf figure 2. The orientational order is then lost. These results clearly confirm what has been said in the previous sections. At temperatures higher than ΔE_1, thermal fluctuations average the tilt angle to zero.

5.2. Confinement regime

The same approach is performed in the confinement regime. Figure 6 displays the absolute value of ζ as a function of γ_{num}. The behaviour is the same as in the previous case. The straight string is stable below the transition and tilts above. However, a jump in the order parameter is noticeable (especially in comparison with the equivalent figure 3 concerning the elastic regime), and this is an indication that the transition is first order. This is further confirmed by looking at the energy displayed in figure 7. It clearly discontinues as a function of γ_{num} at the transition. The numerical study allows us to capture the properties of the charged confined string in the whole range of γ_{num}. This is to be contrasted with the analytical work where we could not consider the small tilt angle region. In contrast with what has been said in [11], this regime is not manifested by an instability of the string towards a modulation. The ground state given by the numerical simulations is also the straight string, either inclined or not.

At finite temperature, the results for the confinement regime are qualitatively the same as for the elastic regime.

6. Applications

6.1. The solitonic lattice (2D)

The present study should be connected, as has been said in the introduction, to previous work on the statistics of solitons. Already, we have considered the domain line as given. Actually, in quasi-1D systems, it has been shown in [11], with the help of a mapping to the ferromagnetic Ising model, that there are no strings, i.e. infinite domain lines of solitons, at non-zero temperature. The latter emerge from a process of exponential growth of aggregates

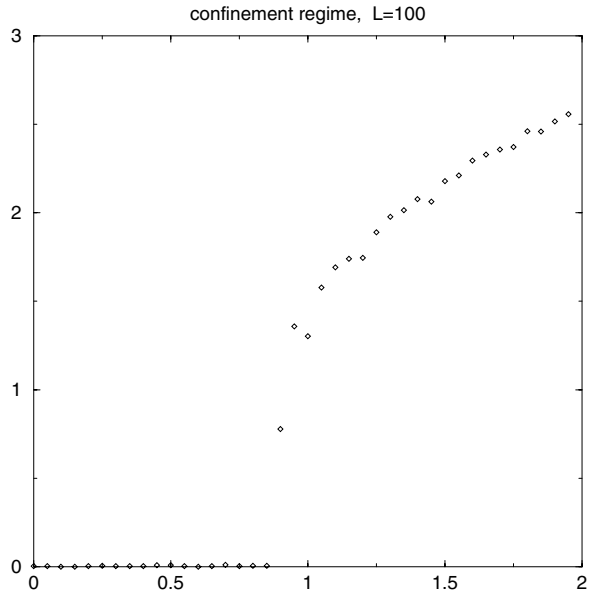

Figure 6. Absolute value of ζ as a function of γ_{num} in the confinement regime.

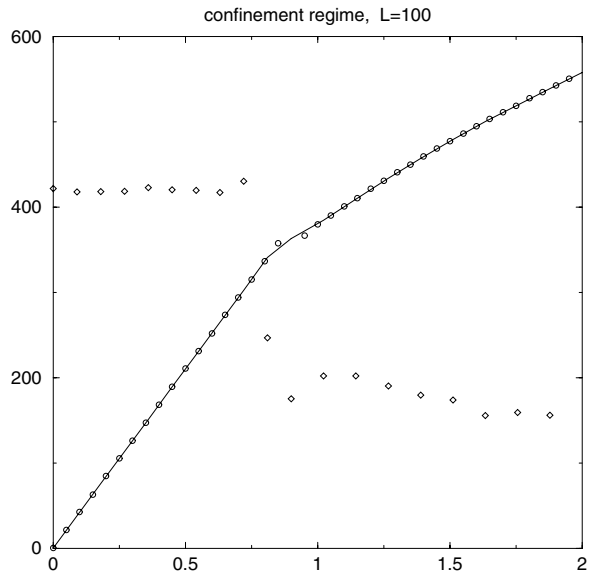

Figure 7. Energy of the string as a function of γ_{num}. The solid curve corresponds to the energy of a string. A discontinuity is clearly noticeable. The diamonds correspond to the first derivative of the latter.

of bisolitons below a crossover temperature T_{cro}. In the non-interacting case, $T_{cro} = T_0$ and the aggregates are finite rods perpendicular to the chains of the quasi-1D system. At zero temperature, the rods cross the whole system forming the free domain lines of solitons. In the interacting case, the crossover temperature is lowered with respect to T_0 and becomes Coulomb dependent. In the region between T_0 and T_{cro}, intrachain antiferromagnetic interactions, within

the ferromagnetic ground state, take place in order for the bisolitons to aggregate, cf [11]. This is due to the important size-charging energy of the aggregates. A crucial approximation is that we have neglected shape instabilities in the interacting case. This reduced us to the region of the phase diagram where $\gamma_D < \gamma_D^c$, cf (20). At high coupling constants, $\gamma_D \gg \gamma_D^c$, strings at $T = 0$, or aggregates at finite temperatures, should melt into a Wigner crystal of solitons. At intermediate coupling constants, the present theory dealing with shape instabilities should be relevant. It should be noted that, in the previous paper, we have suggested that shape instabilities give rise to a modulated string which would correspond to a single negative mode; as we have shown, the instability at intermediate coupling constants is towards a tilt of the interface and affects a continuous set of modes.

Firstly, we seek the stability of the string phase with respect to the Wigner crystal of solitons at $T = 0$. Then we concentrate on the non-zero temperature regime and look for the shape of the aggregates of solitons which lead to strings. To make a comparison with the previous paper easier, notice that the present coupling constant, $\gamma = \gamma_D / \log l_D$, is similar to the coupling constant used in the previous paper Γ. Otherwise we have tried to preserve the same notations.

6.1.1. Zero temperature results: from strings to Wigner crystal of solitons. We define γ_D^{wc} as the coupling constant above which strings melt into a Wigner crystal at $T = 0$. We would like to check here that $\gamma_D^{wc} > \gamma_D^c$ in order to preserve the coherence of the arguments.

As the Coulomb interaction increases, the string of solitons tilts. Its energy also increases. This leads to a dissociation of the string as soon as its energy per soliton $\mu = \delta H^{(0)}/\delta N$ becomes larger than the energy of the constituent soliton μ_{sol}. The latter corresponds to $2J_\perp R/a_x - (ze)^2/\epsilon R$ where $R \approx \sqrt{s/\nu}$ is the radius of the Wigner Seitz cell including the soliton and a background charge of density ν/s with $s = a_x a_y$. This energy can also be written as

$$\mu_{sol} = \frac{2J_\perp R}{a_x}[1 - \nu\gamma]$$

where γ is given by equation (18). The cohesion energy of the string is thus

$$E_c = J_\perp \left(\zeta + \frac{\gamma_D}{\sqrt{1+\zeta^2}} \right) - \mu_{sol}. \tag{37}$$

From equation (37) we see clearly that in the absence of Coulomb interaction, which implies that $\zeta = 0$, the vertical string is stable. When the Coulomb interaction increases, the tilt angle increases beyond the transition to the tilted phase. Thus, E_c increases from negative values. The melting of the string is given by $E_c = 0$ and ζ is the optimal angle of the string, see equation (25). Starting with $\gamma_D \ll 1$ in $E_c = 0$, equation (25) leads to the boundary $\gamma_D = 1/\nu \gg 1$, in contradiction with the starting hypothesis. On the other hand, starting with $\gamma_D \approx 1/\nu$ leads to the lowest boundary $\gamma_D \approx \gamma_D^*$, cf equation (26), again in contradiction with the starting hypothesis. The solution satisfying the self-consistent equation is thus in the intermediate coupling constant range $\gamma_D^* < \gamma_D^{wc} < 1/\nu$ and is given by

$$\gamma_D^{wc} \approx 1/4\nu. \tag{38}$$

We see from equation (38) that, for a sufficiently diluted system, $\gamma_D^{wc} \gg \gamma_D^c$, cf equation (27). The tilted phase might thus be observed when this condition is satisfied.

6.1.2. Non-zero temperature results: shape of the aggregates. More exotic is the case of non-zero temperature. From the point of view of interfaces, these roughen and thus collide at non-zero temperatures. Equivalently, from the point of view of solitons there are no infinite lines but

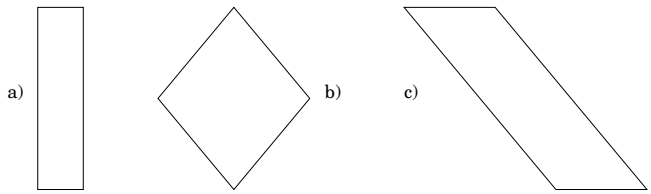

Figure 8. (a) Rod in the absence of Coulomb interaction. The Coulomb energy of (b) is lower than that of (c). At finite temperature the aggregates thus have the shape of (b).

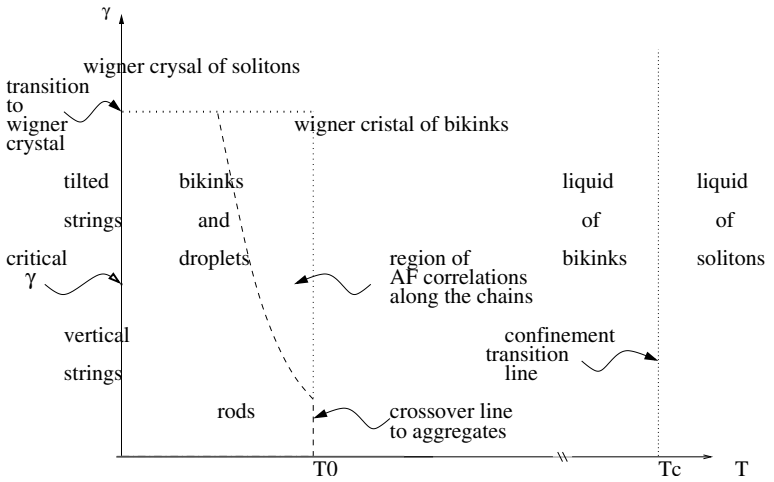

Figure 9. Phase diagram of the 2D system as a function of the coupling constant γ_0 and temperature T. Details are given in the text.

finite size aggregates. The size of the aggregates is approximately given by the distance between two successive collision points of neighbouring interfaces. We address here the question of the shape of the charged aggregates of solitons in the intermediate regime where $\gamma_D^c < \gamma_D \ll \gamma_D^{wc}$. As has already been mentioned, in this regime, the aggregates must adapt their shapes in order to minimize their electrostatic energy. An inclined aggregate, as in figure 8(c), would thus be more favourable than the straight rod. But, at finite temperature, angular kinks are present and they further reduce the Coulomb energy. We can show that a droplet with the shape of figure 8(b) is favoured in comparison with the previous aggregates. This is done by evaluating the energies of these aggregates $\Delta E_b = E_b - E_b^{(se)}$ and $\Delta E_c = E_c - E_c^{(se)}$ where their divergent self-energies $E_b^{(se)}$ and $E_c^{(se)}$ have been subtracted. For the aggregate (c) the separation between the bikinks x_{opt} is taken as the equilibrium separation under the combined action of the Coulomb force $(ze)^2/\epsilon x^2$ and the confinement one $-J_\perp/a_x$, i.e. $x_{opt} = \sqrt{s\gamma}$. Moreover, the tilt angle corresponds to the optimal one. In the confinement regime γ is related to ζ with the help of equation (25). The regularized energies of the aggregates thus depend on one free parameter ζ. The latter must be larger than $1/\sqrt{2}$ to be in the stable confinement regime. We find that the difference between these energies $\Delta E_c - \Delta E_b > 0$ as a function of ζ so that the energy of (b) is always lower than that of (c) above the critical coupling constant γ_D^c.

The results obtained in this section are summarized in the phase diagram figure 9.

6.2. The solitonic lattice (3D)

We consider briefly the important case of 3D systems where interfaces are domain walls. In three dimensions, some rigorous statements allow a good understanding of the uncharged case in the frame of quasi-1D systems, cf [10]. In the presence of Coulomb interactions we thus follow [10] as well as our present experience of the charged 2D case. Concerning notations, in the third direction, z, the coupling constant is taken as J_z and the unit length as a_z.

6.2.1. Uncharged domain wall. For the non-interacting case, it has been shown in [10] that peculiarities are brought about by the rise of dimensionality. In three dimensions, the excitations analogous to rods would be disc-like objects. However, rigorous statements concerning the 3D case show that, at a temperature $T_3 \approx 8J_\perp/\ln(2/\nu) \ll T_c \approx J_\perp/\nu$, a density $\nu_c = \nu - \nu_n$ of solitons condenses into infinite anti-phase domain walls perpendicular to the chains of the quasi-1D system; ν_n then corresponds to the density of finite size solitons below T_3. Therefore, the crossover regime of growing rods, which takes place below T_0 in two dimensions, cannot take place in three dimensions and is replaced by the transition at T_3.

The effect of thermal fluctuations on the walls is well known. Several authors have shown (see references in [16]) that, in three dimensions the height–height correlation function remains finite at $T < T_R$ whereas it diverges logarithmically for $T \geqslant T_R$, where $T_R > 0$ is the roughening temperature. From these considerations, T_3 may be considered as the roughening temperature. The existence of walls in three dimensions at finite temperatures is compatible with the fact that in Ising-like systems there is 2D long-range order at low temperatures.

6.2.2. Charged domain wall versus Wigner crystal. The 3D case of charged walls can be treated in the same way as the 2D case. We therefore consider again the elastic and confinement regimes. The Coulomb interaction will lead to a tilting of the wall here also. Two tilt angles can be defined now, because the anisotropy axis becomes an anisotropy plane. We thus consider ζ_y which corresponds to the previous, in-plane, tilt angle and ζ_z which is the tilt angle with respect to the third direction. The mean-field Hamiltonian of the system is then

$$H_p/J_y = \zeta_y^{p_y} + \alpha_\perp \zeta_z^{p_z} + \gamma_D \left[\frac{1}{\sqrt{1+\zeta_z^2}} \left(1 - \frac{1}{2} \log\left(\frac{1+\zeta_y^2}{1+\zeta_z^2} \right) \right) - 1 \right] \tag{39}$$

where $\alpha_\perp = J_z/J_y$, $\gamma_D = e^2 l_D/\epsilon s_\perp J_y$, $s_\perp = a_y a_z$ and, in the last term, the contribution of the straight domain wall has been subtracted. Notice that it is only in the case where $\zeta_y = \zeta_z = \zeta$ that we gain a global factor $1/\sqrt{1+\zeta^2}$ as in the 2D case. The logarithm is therefore the signature of a non-homogeneous charge dilatation within the wall.

Our aim is to determine the phase diagram, γ_D versus $\alpha_\perp$ in both regimes, i.e. $p_{y,z} = 1, 2$. Among the four possible cases, we consider only the full elastic ($p_y = p_z = 2$) and mixed ($p_y = 2$, $p_z = 1$) regimes.

In the elastic regime, $p_y = p_z = 2$, the phase diagram is displayed in figure 10. For $\gamma_D > 2\alpha_\perp$, the stable solution is given by

$$\zeta_y = \zeta_z = 0. \tag{40}$$

In the region $\gamma_D < 2\alpha_\perp$, the stable solution corresponds to

$$\zeta_y = 0 \qquad \zeta_z = \sqrt{\frac{\gamma_D}{2\alpha_\perp} - 1}. \tag{41}$$

For $\gamma_D^s \approx 16 < \gamma_D < (2\alpha_\perp)^{3/2}\sqrt{\log \alpha_\perp/4}$ a third phase, corresponding to

$$\zeta_y \approx \left(\frac{\gamma_D}{6} \log\left(\frac{\gamma_D}{4} \right) \right)^{1/3} \qquad \zeta_z = 0 \tag{42}$$

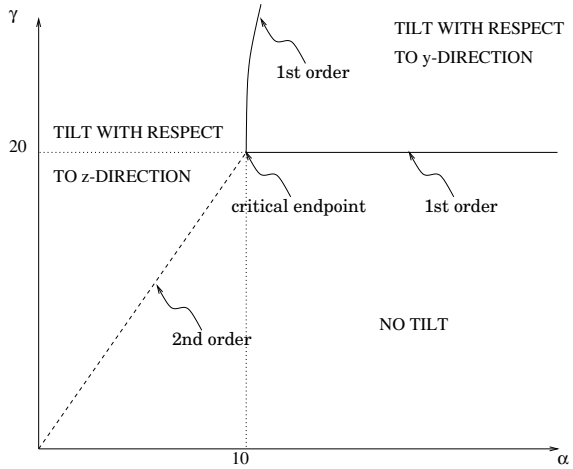

Figure 10. Phase diagram of the elastic wall: γ_D as a function of $\alpha_\perp$.

is stable. The domain of validity of this solution overlaps those of the two previous solutions. With the help of energetic considerations, we find that a line of first-order critical points, at $\gamma_D \approx 20$, separates phase (40) from phase (42). In the same way, a line of first-order critical points has been found to separate phase (41) from phase (42). The line $\gamma_D = 2\alpha_\perp$ is a line of second-order critical points which terminates at the critical end-point $\alpha_\perp = 10$, $\gamma_D = 20$. Phases which have both angles non-zero appear to be unstable.

A similar analysis can be done for quasi-two-dimensional (Q2D) systems where the interface is elastic within the planes, i.e. $p_y = 2$ and in the confinement regime between planes, i.e. $p_z = 1$. For Q2D systems, the coupling in the third direction is weak with respect to the coupling in other directions, i.e. $\alpha_\perp < 1$. In the region of the phase diagram where $\alpha_\perp < 1$, the solution is thus given by

$$\zeta_y = 0 \qquad \zeta_z = \frac{\gamma_D}{2\alpha_\perp} + \sqrt{\left(\frac{\gamma_D}{2\alpha_\perp}\right)^2 - 1} \tag{43}$$

and is stable for $\gamma_D > 2\alpha_\perp$. As before, when $\gamma_D < 2\alpha_\perp$, the untilted solution is stable for small $\alpha_\perp$ and is separated from the previous by a line of second-order critical points. From equations (41) and (43), we see that for a given value of the ratio $\gamma_D/2\alpha_\perp$, the tilt is stronger in the mixed regime than in the pure elastic regime. This can be interpreted by considering the equilibrium position of a constituent of the wall due to the constant confinement force and the constant electric force due to the charged wall; a priori, the equilibrium is reached only at $\gamma_D = \alpha_\perp$, a feature which is peculiar to the confinement regime. This implies that the wall should melt as soon as $\gamma_D > \alpha_\perp$ or, if the Coulomb energy scale is sufficiently weak, that the wall should strongly incline to reduce the coupling constant. Allowing the wall to tilt, the equilibrium equation, $\gamma_D = \alpha_\perp$, is generalized to

$$\frac{\gamma_D}{\alpha_\perp}\left(1 - \frac{1}{2}\log(1+\zeta_z^2)\right) = 1.$$

which leads to the following minimal stability angle

$$\zeta_z = \exp\left(2\left(1 - \frac{\alpha_\perp}{\gamma_D}\right)\right) - 1$$

above which the wall stabilizes at the equilibrium angle (43).

In three dimensions, the situation is thus richer than in the 2D case with the appearance of a tricritical point and quantitative differences between the various regimes but, qualitatively, the same phase diagram for all of them. In particular, the tilting of the interface takes place with respect to a single anisotropy axis and not both. In Q2D systems, the wall should tilt with respect to the third direction rather than the y-direction and the tilting is stronger in the confinement regime to prevent the melting. Another difference with the 2D case is that thermal fluctuations do not affect these results, as long as we are below the roughening temperature of the wall.

6.3. Stripes in oxides

Up to now, the whole theory is model independent. As we have already mentioned, our results could be applied to doubly commensurate CDWs such as polyacetylene. However, we consider physical systems which are quite extensively studied nowadays. These are the oxides, e.g. cuprate, nickelate, manganese and the new ferroelectric state. The latter is considered in the next section. Here we focus on the phenomenology of stripes with the help of the above theory. We concentrate only on the long distance properties, namely, the fact that stripes consist of lines or walls of holons which are similar to the charged solitons we have been considering. The latter are thus charged interfaces as those described in this paper.

The oxides we consider are Q2D materials formed by coupled planes. At intermediate values of doping, a 3D ordering of the stripes might have been seen in $La_{1.6-x}Nd_{0.4}Sr_xCuO_4$ and $La_{2-x}Sr_xNiO_{4+\delta}$, cf [5] and references therein. The impact of the pinning by the lattice and the Coulomb interactions play a crucial role in these systems.

In $La_{1.6-x}Nd_{0.4}Sr_xCuO_4$ neutron diffraction studies have revealed diffuse magnetic peaks along the z-direction, in the stripe phase, which is consistent with stripes as 1D interfaces. Moreover, x-ray studies reveal that stripes are parallel in next-nearest-neighbouring layers but orthogonal between nearest layers. This 3D ordering is probably due to a pinning of the stripes by the lattice structure.

The case of nickelates is more interesting. In $La_{2-x}Sr_xNiO_{4+\delta}$ there is a body-centred stacking of parallel elastic stripes with only weak perturbations due to the lattice. This 3D ordering is due to Coulomb repulsion and might correspond to a domain wall with a step-like profile suggesting a confinement regime in the third direction. This justifies the mixed confinement–elastic regime we have considered in section 6.2. Experimental results do not however exclude the interpretation of this 3D ordering as a Wigner crystal of lines. The latter hypothesis allows us to focus on strings within planes of the Q2D system.

Following Wakimoto *et al* [7], we recall briefly here some experimental results related to the tilting of string-like stripes in $La_{2-x}Sr_xCuO_4$.

The experimental results are summarized in figure 11 which has been taken from [7]. In figure 11(a), $\delta = 2\pi/d$ where d is the distance between stripes. At low doping, the inset on the left of this figure shows magnetic Bragg peaks corresponding to a 1D spin modulation which is inclined with respect to the reference tetragonal axis. At higher doping, the inset on the left shows that this spin modulation and the charge stripes have rotated by an angle of 45°. The main figure and figure 11(b), which displays the tilt angle as a function of the concentration of dopant, show that this shape instability takes place around $x_c \approx 0.05$ where δ increases linearly with x. Moreover, the authors report a weak dependence of the magnetic peaks on the third direction. This implies that the spin modulations are weakly correlated between successive CuO_2 layers. Thus, the stripes can be considered with as good an accuracy as charged strings, which justifies our starting hypothesis.

The stripe instability observed experimentally might be due to the competition between the long-range Coulomb interaction and an anisotropic interaction. To relate this instability to

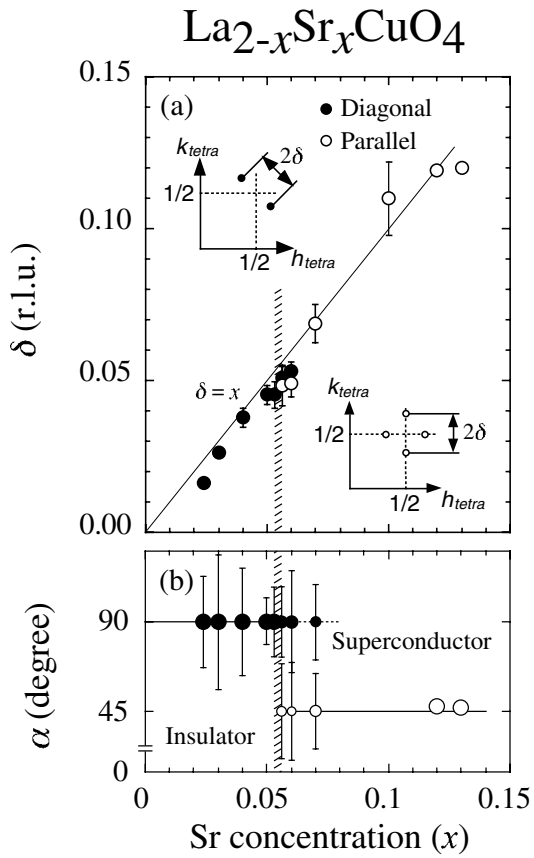

Figure 11. Tilting of stripes in a cuprate oxide (from [7]).

an increase of the concentration of dopants x, we should probably take into account structural changes. As argued by Tranquada *et al* [5], the lines of charge might be pinned along the direction of the tilt of the CuO_6 octahedron. This tilt direction varies with doping. It is along the orthorhombic axis at low doping and along the tetragonal axis at higher doping. These axes are 45° from each other. At an intermediate doping, corresponding to the critical value x_c, a 45° tilt of the stripes, satisfying the structural constraints, can take place.

Simple considerations related to the competing energy scales are in favour of such an order of magnitude for the tilt angle. Firstly, in this system $e^2/\epsilon a \sim 0.1$–1 eV where a is a unit length of the tetragonal structure. Secondly, the exchange energy $J_\perp$ is of the order of 0.13 eV. Thus, $\gamma \sim 0.4$–4.5 where equation (18) has been used. If we consider that the Debye length is of the order of the inter-stripe distance $1/\delta$, at the transition x_c we have $l_D \sim 20a$. Thus, $\gamma_D = \gamma \ln(l_D/a) \sim 1.2$–13.5. Using equation (21), the maximum tilt angle compatible with these values is around 55°. A tilt angle of 45° can be reached with $\gamma_D \sim 4.0$ which is clearly in the range of the allowed values. Hence, the competing interactions can be responsible for such a tilt.

This tilt could reduce the electrostatic energy of the stripe as can be seen by the following argument. At low doping, i.e. in the diagonal stripe phase, the hole concentration along the stripe is 0.7 hole/Cu. This concentration is reduced to 0.5 hole/Cu in the collinear stripe phase, cf Wakimoto *et al*. The density of charges along the stripe is thus reduced by $\sqrt{1+\zeta^2}$, with

$\zeta = 1$ for the present 45° tilt angle. This dilatation factor reduces the electrostatic energy of the string as has already been seen in equation (19). This could hold assuming that the number of holes per stripe is constant. The added dopants would lead to the formation of new stripes. The latter become tightly packed at high doping as suggested by the linear relation $\delta \approx x$.

6.4. Uniaxial ferroelectrics

Recently, a ferroelectric Mott–Hubbard state has been observed in quasi-1D organic superconductors such as $(TMTTF)_2X$. We give a brief account of the origin of this phase and connect the results to our present study. Experimental and theoretical results are given in detail in [4].

In the system mentioned above $TMTTF$ are molecules composing the stacks and therefore giving rise to the 1D nature of the compound. X are ions placed in the vicinity of the molecules. At large temperatures, of the order of 100 K, the ions reorder through a uniform shift which gives rise to a ferroelectric phase. The latter has been detected via the measurement of the dielectric susceptibility which shows a gigantic anomaly at low frequency around $T_{fe} \sim 150$ K. At low-temperature domain lines, separating domains with opposite polarization should be observed. Their existence is necessary to minimize the external electric field generated by charges accumulating at the boundary of the sample. Moreover, as the interface corresponds to a jump in the polarization it is charged. Following [4] we define as α solitons the elementary constituents of the interface which connect domains with opposite polarization. They carry a fractional charge ze with $z = 2\alpha/\pi$.

Two facts suggest that this system is a good candidate for the observation of charged interfaces. Firstly, the background dielectric susceptibility $\epsilon_0 \sim (\omega_p/\Delta)^2 \sim 10^4$ is large. Furthermore, π solitons are also present and they screen the Coulomb interaction. This weakens the Coulomb interaction. In such systems, the strings of α solitons should thus be stable against a melting towards a Wigner crystal. Bubble-like aggregates of α solitons, such as those described in section 6.1, could also be observed at higher temperatures.

7. Conclusion

The statistics of charged interfaces, strings and walls has been studied. We have found that shape instabilities, due to competing interactions, play a fundamental role. They manifest themselves through zero-temperature phase transitions from which new ground states emerge where the interface is tilted. The 2D case of the string has been extensively studied. For small tilt angles, the string is elastic and the transition to the tilted ground state is second order. On the other hand, a first-order transition takes place if we are beyond the limit of validity of the elastic regime, i.e. in the confinement regime. At non-zero temperatures it has been shown that in either regime a pure Coulomb roughening of the string, due to the proliferation of angular bikinks, exists in addition to the usual roughening as soon as $T > 0$. At higher temperatures angular kinks are thermally activated and connect the degenerate ground states. These results have been confirmed with the help of a numerical approach based on the Monte Carlo–Metropolis algorithm. We have then related the present study to the general problem of the statistics of solitons in CDW systems in either two or three dimensions. In 2D systems, the string has been shown to emerge from bubble-like aggregates of solitons upon decreasing temperature. In 3D systems, the additional coupling constant in the third direction enriches the tilted phases with the appearance of a tricritical point separating them. In the confinement regime, a disintegration of the wall is favoured but the solitons might order in the form of a strongly inclined wall. Applications concerning stripes in oxides and a possible explanation

of their tilt, as well as charged strings in uniaxial ferroelectric experiments, have also been considered.

Acknowledgments

I would like to thank S Brazovskii for helpful and inspiring discussions from the very beginning of this work. I would like to thank A Bishop for numerous discussions and his hospitality at the Theoretical Division and Center of Non-Linear Studies, Los Alamos.

Appendix A

In this appendix we give some details on the screening in the ensemble of solitons. Screening makes the energy extensive and gives a meaning to the thermodynamic limit, as has been said throughout the paper. In the following, we work in the RPA approximation which is very well known in the field of many-body theory. This allows us to derive the Debye length and the electrostatic potential in two cases: 2D and 3D screening.

We consider first a single plane embedded in 3D space. This case corresponds to 2D screening. Supposing that the Coulomb field ϕ is slowly varying, it obeys the following semi-classical equation

$$-\epsilon\Delta\phi(\vec{R}) = -4\pi e^2(\Pi^{(0)} * \phi)(\vec{R})\delta(z) + 4\pi e^2\rho_0(\vec{r})\delta(z) \tag{44}$$

where $\vec{R}$ is a 3D vector associated with the 3D Coulomb field, $\vec{r}$ is a 2D vector indexing the charges which are embedded in the $z = 0$ plane and ρ_0 is some external charge. $\Pi^{(0)}(x, y)$ is the response function, or polarization part, of the soliton system which is related to the correlation function by the fluctuation dissipation theorem

$$T\Pi^{(0)}(\vec{r}) = \langle\delta\rho(\vec{r})\delta\rho(\vec{0})\rangle \tag{45}$$

where $\delta\rho(\vec{r}) = \rho(\vec{r}) - \nu$, with $\rho(\vec{r})$ being the density of solitons and ν the background neutralizing charge.

The first term on the right-hand side of equation (44) corresponds to the screening charge. this term implies linear screening and dispersion via the convolution. The Coulomb field is then

$$\phi(\vec{k}, z = 0) = \frac{2\pi e^2\rho_0(\vec{k})}{\epsilon|k| + 2\pi e^2\Pi^{(0)}(\vec{k}, z = 0)} \tag{46}$$

where $\vec{k}$ is the reciprocal vector associated with $\vec{r}$. The fact that the potential is evaluated at $z = 0$ implies that the field lines are confined to the same space as the particles, cf [17]. Expression (46) leads to the Debye screening of the field with a Debye length

$$\frac{1}{l_{2D}} = \frac{2\pi e^2}{\epsilon}\Pi^{(0)}(k = 0). \tag{47}$$

Also, the k-term in the denominator of equation (46) is a feature of 2D systems. In real space, this leads to an algebraic screening instead of the exponential screening; cf [17] for detailed studies of screening effects in Coulomb fluids, and also see the following example.

We consider now the 3D case of independent planes embedded in a neutral medium. Such a system of decoupled planes brings a 3D screening. The screening charge is then a function of the 3D vector $\vec{R}$. But, as the planes are independent, the bare correlation function corresponds

to $\Pi^{(0)}(\vec{R}) = \Pi^{(0)}(\vec{r})\delta(z)$. Using the same arguments as in the first section, we can compute the Coulomb field which reads

$$\phi_{3D}(\vec{K}) = \frac{4\pi e^2 \rho_0(\vec{K})}{\epsilon K^2 + 4\pi e^2 \Pi^{(0)}(\vec{k}, z = 0)/a_z} \tag{48}$$

where we consider only the $z = 0$ plane subject to the bulk screening. The 3D Debye length is then given by

$$\frac{1}{l_{3D}^2} = \frac{4\pi e^2}{\epsilon a_z} \Pi^{(0)}(k = 0) \tag{49}$$

where a_z is the inter-plane distance. In real space, equation (48) leads to the usual exponential screening.

Finally we derive the polarization part for the present problem. This gives explicit expressions for the screening lengths and for $\phi(\vec{r})$. Below the crossover transition T_0

$$T\Pi^{(0)}(x, y) \approx \frac{1}{2s^2} \nu a_x \exp\left(-\frac{2y}{l_\perp}\right)(2\delta(x) + \delta(x + a_x) + \delta(x - a_x)) \tag{50}$$

corresponding to the aggregation of the solitons into rods of length $l_\perp$, cf [10]. Fourier transforming equation (50) we obtain

$$T\Pi^{(0)}(\vec{k}) \approx \frac{\nu}{4sa_y}(1 + \cos(k_x a_x)) \frac{l_\perp}{1 + k_y^2 l_\perp^2/4}.$$

Thus $\Pi^{(0)}(\vec{k}) \approx \frac{\nu l_\perp}{2sa_y T}$ and, as we work at constant density of solitons $\nu, l_\perp \approx \sqrt{2\nu}\exp(2J_\perp/T)$. With the help of equations (47) and (49), this yields

$$l_{2D} = \frac{2\epsilon s a_y T}{\pi e^2 (2\nu)^{3/2}} \exp\left(-\frac{2J_\perp}{T}\right) \qquad l_{3D} = \sqrt{\frac{\epsilon s a_z T}{\pi e^2 (2\nu)^{3/2}}} \exp\left(-\frac{J_\perp}{T}\right). \tag{51}$$

In the 2D screening regime, the field can then be written, in the long distance limit with respect to the coarse-graining length a_x

$$\phi(\vec{k}) = \frac{2\pi e^2}{\epsilon} \frac{1 + k_y^2 l_\perp^2/4}{|k|(1 + k_y^2 l_\perp^2/4) + 1/l_D} \tag{52}$$

which reflects the anisotropy of the problem. To give an idea of the algebraic screening, we Fourier transform equation (52) in the limit $k_y l_\perp \to 0$, i.e. far enough from the rod. This yields

$$\phi(\vec{r}) \approx \frac{2\pi e^2}{\epsilon} \frac{l_D^2}{r^3}$$

in the limit $r \gg l_D$. We see that the algebraic tail leads to a slow decay of the potential in contrast to the usual exponential decay. However, this type of interaction beyond the screening length as well as the dipolar-type interaction are compatible with the growth of the aggregates, cf [11]. See [19] for more details concerning screening in this system.

Appendix B

Our purpose is mainly to show the differences and common points between the two interface models. The approach is based on the transfer matrix method. In the present case, this formulation cannot be used straightforwardly because of the long-range interactions in equation (10). Some results obtained in the non-interacting case should however remain in the presence of the long-range interaction. It is on such a property that we now focus.

The associated Hamiltonian of the problem is

$$\beta H_p = \frac{K}{a^{p-1}} \sum_{y=0}^{L-1} |x_{y+1} - x_y|^p \tag{53}$$

where the short distance cut-off has been taken explicitly into account. The transfer matrix $\hat{T}_a$ is defined as an integral operator with eigenfunctions $\psi(x)$ whose kernel is expressed in terms of equation (53). Namely

$$\hat{T}_a \psi(x) = \int \mathrm{d}x' \exp\left(-\frac{K}{a^{p-1}}|x - x'|^p\right)\psi(x'). \tag{54}$$

The free problem is simple enough to be treated just with the integral equation (54). For a more exhaustive account of the general results one can obtain with help of the transfer matrix method, see [18], which deals with the problem of an elastic string in an external potential.

For both models, the eigenfunctions of the transfer matrix are simply plane waves

$$\psi_k(x) \approx \exp(\mathrm{i}kx).$$

This amounts to Fourier transforming the kernel of equation (54). The eigenvalues of the transfer matrix associated to both interface models are thus

$$\epsilon_k^G \approx \frac{k^2}{2K} \qquad \epsilon_k^{SOS} \approx \log(K^2 + k^2). \tag{55}$$

By comparing the two spectra in equation (55) we see clearly that both models have the same long distance, i.e. $k \to 0$, properties.

References

[1] Brazovskii S and Kirova N 1984 *Physics (Soviet Scientific Reviews Section A)* vol 5, ed I M Khalatnikov (New York: Harwood Academic) p 99
[2] Yu Lu 1988 *Solitons and Polarons in Conducting Polymers* (Singapore: World Scientific)
[3] Heeger A J, Kivelson S and Schrieffer J R 1988 *Rev. Mod. Phys.* **60** 781
[4] Monceau P, Ya Nad F and Brazovskii S 2001 *Phys. Rev. Lett.* **86** 4080
[5] Tranquada J M 1998 *Neutron Scattering in Layered Copper Oxide Superconductors* ed A Furrer (Dordrecht: Kluwer)
[6] Bosch M, van Saarloos W and Zaanen J 2001 *Phys. Rev.* B **63** 092501
[7] Wakimoto S *et al* 2000 *Phys. Rev.* B **61** 4326
Fujita M *et al* 2002 *Phys. Rev.* B **65** 064505
[8] Dai P *et al* 2000 *Phys. Rev. Lett.* **85** 2553
[9] Schon J H, Berg S, Kloc Ch and Battlogg B 2000 *Science* **287** 1022
[10] Bohr T and Brazovskii S 1983 *J. Phys. C: Solid State Phys.* **16** 1189
[11] Teber S, Stojkovic B P, Brazovskii S A and Bishop A R 2001 *J. Phys.: Condens. Matter* **13** 4015–31
[12] Kantor Y and Kardar M 1989 *Europhys. Lett.* **9** 53
[13] Netz R and Orland H 1999 *Eur. Phys. J.* B **8** 81
[14] Lee P A, Rice T M and Anderson P W 1974 *Solid State Commun.* **14** 703
[15] Rice M J, Bishop A R, Krumhansl J A and Trullinger S E 1976 *Phys. Rev. Lett.* **36** 432
[16] Forgacs G *et al* 1991 *Phase Transitions and Critical Phenomena* vol 14, ed C Domb and J L Lebowitz (London: Academic)
[17] Cornu F 1998 *Thèse d'habilitation*
Cornu F 1996 *Phys. Rev.* E **53** 4595
Jancovici B 1995 *J. Stat. Phys.* **80** 445
[18] Suris R A 1965 *Sov. Phys.–JETP* **20** 961
[19] Teber S 2002 *Thése de doctorat*